Original Paper

Evaluation of formation damages during filter cake deposition and removal process: The effect of primary damage on secondary damage

Jaber Al Jaberi [a], Badr S. Bageri [a, *], Abdulrauf R. Adebayo [b], Shirish Patil [a], Assad Barri [a], Rahul B. Salin [b]

[a] Department of Petroleum Engineering, King Fahd University of Petroleum & Minerals, Dhahran, 31261, Saudi Arabia
[b] Center for Integrative Petroleum Research, King Fahd University of Petroleum & Minerals, Dhahran, 31261, Saudi Arabia

A R T I C L E   I N F O

A B S T R A C T

The properties of oil and gas formation could be significantly damaged during drilling and completion operations as a result of mud invasion, fluid incompatibility and interaction with rock minerals. This paper presents a systematic method for evaluating formation damage during filter cake deposition (primary damage) and removal process (secondary damage). The role of primary damage in the evolution of secondary damage was also investigated. The interaction of the filter cake solvent (chelating agent solution) with the rock samples was implemented through core flooding experiment. Nuclear Magnetic Resonance (NMR) was used to evaluate the properties of the rock sample, pre and post filter cake deposition and removal processes. The results show that secondary damaged is a strong function of the location and the intensity of the primary damage. The rock type and its pore structure also play important roles in both primary and secondary damage. The extent of secondary damage depends on the amount of barium sulphate deposited during primary damage. The chelating agent used to dissolve the barites in sandstones, deposited the barite in the small pores while it enlarges the bigger pores. In contrast, the chelating agent in the carbonate samples had multiple barite deposition points.

1. Introduction

Formation damage can be defined in the petroleum industry as an impairment of oil and gas reservoir formation properties caused by particle retention, fluid invasion and interaction. Formation damage has a negative impact on well deliverability, stability, economics, environment, and in some cases human health. The formation damage is caused by chemical and physical interactions between the fluid and the formation which alters the pores and minimize flow conductivity (Nunes et al., 2010; Bageri and Mahmoud, 2013; Liu et al., 2013; Al-Yaseri et al., 2015; Zhao et al., 2019; Ding et al., 2020). Formation damage is an undesirable and challenging problem that can occur during different development phases of oil and gas wells such as drilling, completion, injection, and workover operations. Formation damage can be classified into two types based on the cause of the damage namely primary and secondary damage. Primary and secondary formation damage can be caused during filter cake formation and removal processes, respectively. The complete process of filter cake formation, filter cake removal, and the associated formation damage in the field is illustrated in Fig. 1.

1.1. Primary formation damage

Primary formation damage, referred to as Stage 1 in Fig. 1, occurs during overbalanced drilling operations, when the filter cake starts to form. During this stage, the solid particles in the drilling mud deposit on the formation face due to the filtration process resulting in the formation of filter cake (Zhong et al., 2019; Bageri et al., 2020). Nonetheless, the tiny solid particles in the drilling fluid may penetrate the filter cake and invade the drilled formation. The invaded particles then plug part of the pores causing a primary formation damage (Iscan et al., 2007; Fattah and Lashin, 2016; Ettehadi and Altun, 2017; Basnayaka et al., 2018). Forming a thin and impermeable filter cake layer is one of the functions of drilling fluids in order to minimize formation damage (Hodge et al., 1997;
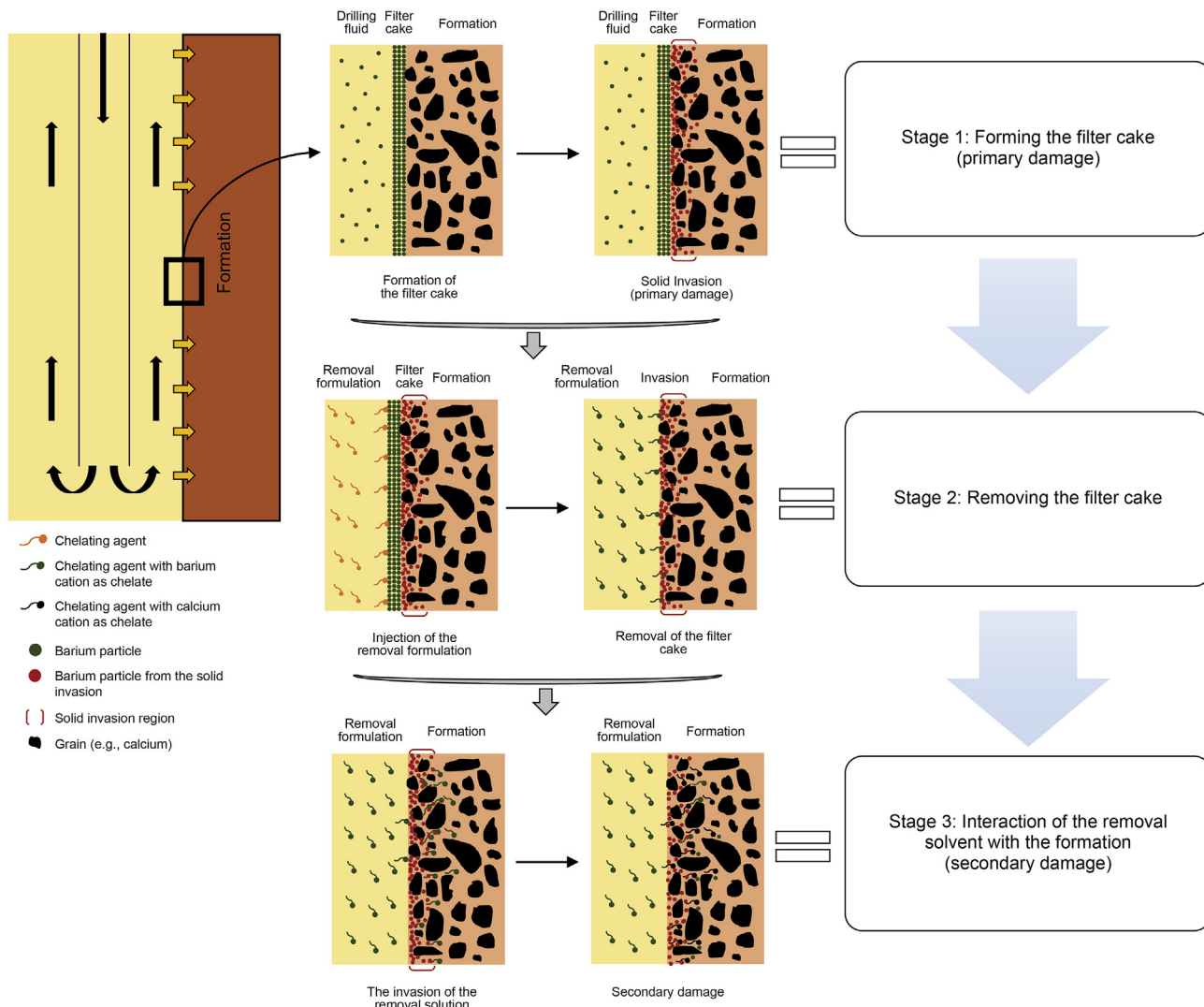
Fig. 1. Schematic showing various stages of formation damage during drilling and post drilling cleanup operations.

Khodja et al., 2010; Bageri et al., 2020). Hence, researchers have been working tirelessly to enhance the properties of drilling fluids using different additives and techniques (Yue and Ma, 2008; Zhang et al., 2009; Qiansheng et al., 2010; Wang et al., 2012; Ahmad et al., 2018; Mahmoud et al., 2018; Smith et al., 2018; Sun et al., 2018; Bageri et al., 2020; Guancheng et al., 2020).

Further challenges are faced as drilling operation advances to deeper oil and gas wells due to high pressure and temperature conditions. These conditions lead to deterioration of fluid performance necessitating the use of additives with improved ability to withstand the high-temperature (Mao et al., 2020). The high-pressure conditions, on the other hand, require the use of high-density weighting agent such as barite and calcite (Hossain and Al-Majed, 2015). It is therefore important to assess how these different additives impact the filter cake properties such as permeability, porosity, composition, and thickness.

To date, many techniques have been implemented to analyze filter cake properties such as gravimetric method, X-ray computed tomography scan (CT scan), scanning electron microscopy (SEM), and laser diffraction method (Bageri et al., 2013; Byrne et al., 2000; Elkatatny et al., 2011; Green et al., 2013; Al Moajil et al., 2008; Al Otaibi et al., 2008). Nuclear magnetic resonance (NMR) emerges as a new promising method to evaluate filter cake properties and

formation damage (Adebayo and Bageri, 2019; Adebayo et al., 2020). What makes the NMR technique superior compared to the other methods is the following advantages: minimal sample handling needed and the possibility to be applied in the field during drilling operations.

1.2. Filter cake removal

To recover the formation hydraulic conductivity after drilling operations, the deposited filter cake on the borehole wall has to be removed mechanically or chemically (referred to as Stage 2 in Fig. 1) (Al-Mutairi and Al-Dhufairi, 2010). Since weighting agents constitute about 80%–90% of the filter cake, the removal solution must be able to dissolve them (Mahmoud et al., 2017). Therefore, various chemical removal methods of removing filter cake particles have been vastly researched with extensive guidelines provided for filter cake treatment in oil and gas wells. Different chemicals were recommended to dissolve filter cake layer including chelating agents, acids, oxidizers, enzymes, emulsion, and various other chemicals (Bageri et al., 2017; Al Moajil and Nasr-El-Din, 2014; Wanderley Neto et al., 2020) All these filter cake dissolving chemicals can efficiently dissolve barite and calcite filer cakes. In particular, chelating agent solutions such as diethylenetriaminepentaacetic

acid (DTPA) and ethylenediaminetetraacetic acid (EDTA) are unique solvents due to their good adsorption capacity of metal-containing materials, their stability at high temperature, and low environmental impact (Barri et al., 2016; Elsayed et al., 2020; Fredd and Fogler, 1998; Mahmoud et al., 2018a). Moreover, the use of polymer as additive in drilling fluid can create a coating layer on the weighting particles, which might dampen the reaction between the removal solution and the filter cake component (Al Moajil et al., 2008). This then calls for another chemical called polymer breaker required to dissolve the coating layer and then allowing the removal solution to react with the filter cake (Siddiqui and Nasr-El-Din, 2003). Based on the compatibility between the different removal solution components, the removal process could be a single stage or multi stages processes (Mahmoud, 2019). Single stage refers to stage where both the polymer breaker and the filter cake removal solutions are combined, while the multi-stage removal process refers to separately breaking the polymers with one chemical solution and then subsequently dissolving the filter cake with another solution.

1.3. Secondary formation damage

Secondary formation damage is a relatively new term that can describe the formation damage caused after or during the filter cake removal process. It can be induced by the incompatibility of the removal solvent with the formation fluid or the solvent potential to react with formation minerals (Bageri et al., 2019; Al Jaberi et al., 2020; Al Moajil and Nasr-El-Din, 2013; Al Moajil and Nasr-El-Din, 2011; Nasr-El-Din, 2005). Recently, it has been (Bageri et al., 2019) shown, using the NMR technique, that the chelating agent solution, used for barite filter cake removal process, interacted with the clay minerals in sandstone formations and calcite matrix during filter cake removal process. The saturated barium chelating agent can introduce a new damage to the formation (Bageri et al., 2019). The interaction was investigated by injecting a chelating agent solution into sandstone and carbonate formation rock samples (100% saturated with brine). Their result explained the interaction mechanism in both sandstone and carbonate formations. This work mainly focused on the chemical interaction between the core sample and the chelating agents without considering the effect of primary damage. The work was simplified to examine the interaction (Bageri et al., 2019), where the filter cake deposition stage prior to the interaction between the rock and chelating agent was not thoroughly considered. Therefore, it is important and interesting to extend this work and conduct some additional research on the mechanism of primary damage to explore its effect on the secondary damage formation. This is still one of the most important ways to discuss the intrinsic damage stage that controls change in the formation properties during filter cake deposition and removal processes.

1.4. Emerging methodology to characterize secondary formation damage

Since the concept of secondary damage is recent, a clear methodology is needed to evaluate secondary damage. This is achieved by the following steps that can be conducted to simulate downhole conditions as shown in Fig. 1.

Step-1: The objective of this step is to simulate in the laboratory the primary damage stage and obtain a representative filter cake sample over a rock sample (core sample) using the fluid loss test. The test conditions depend on the formation temperature and the overbalance pressure (usually 300 to 500 psi) applied for a specific time (standard API test is 30 min). The evaluation of primary damage can involve the use of different indices such as measuring

the reduction in porosity and permeability of core samples, depth of invasion, and concentration of the invaded solids. The properties of core samples are measured before and after the filtration test using NMR to assess the concentration of the invasion and measure the volume of the pores filled with the invaded solids. At the end of this stage, the change in the core sample properties as result of filter cake deposition are measured.

Step-2: The conventional practice to measure the filter cake removal efficiency is applied by placing the formed filter cake with rock sample (Step-1) in the filtration cell (Step-2: Approach-1). This procedure requires filling the filtration cell with the designed filter cake removal fluid (chelating agent for barite filter cake). The time of the removal test depends on the effective removal time of the solvent. It was found to be 24 h in the barite filter cake removal process. After the removal of the filter cake (i.e., barite filter cake), the removal fluid is saturated with the weighting material of filter cake (barite). NMR measurement for the filter cake and filtration properties requires removal of the filter cake from the top of the core sample. An alternative approach to remove the filter cake (i.e., Step-2: Approach-2) is to saturate the removal fluid with the filter cake weighting material (barite) using a solubility apparatus. The formed filter cake solids are dissolved in the removal fluid under the same temperature and at an effective removal time (24 h). At the end of this step, the solvent saturated with filter cake solids can be obtained.

Step-3: The objective of this step is to allow the removal fluid (saturated with filter cake) penetrate the core sample. There are two approaches to ensure rock–infiltrated fluid interaction and evaluate the secondary damage; the first approach (Step-3: Approach-1) is to run the removal process for longer time than the effective time of the filter cake removal as shown in (Step-2: Approach-1). To get a representative data, the formed filter cake (Step-1) must be dissolved completely (Step-2: Approach-1) to ensure that removal fluid penetrate the formation rock sample. On the other hand, if the filter cake was not removed completely, the remaining particles of the filter cake may restrict the penetration of the removal fluid and lead to incomplete evaluation of the secondary damage, making it a time-consuming process. Hence, Bageri et al., (2020) proposed alternative approach (Step-3: Approach 2) by using the core flooding system to inject the removal fluid into the core sample. This approach is compatible with the second approach in the second step (Step-2: Approach 2), where the formed filter cake removed from the top of the core sample and dissolved in the removal fluid separately using solubility apparatus.

In summary, the first step (Step-1) is to form the filter cake using the fluid loss test. After which, the formed filter cake is dissolved in the removal fluid using the solubility apparatus in the second step (Step-2), in order to saturate the removal fluid with the filter cake weighting agent. Finally, the removal fluid (saturated with filter cake weighting agent) is injected into the core sample using the core flooding system to evaluate the secondary damage. NMR technique must be implemented before and after the first and last steps (Step-1 and Step-3) to evaluate the primary and secondary damages, respectively.

In this study, the methodology explained previously was implemented with all the steps to honor the mud invasion and rock-fluid interaction sequence in the presence of filter cake as depicted in Fig. 1, which represents the actual field scenario. It is identified that the presence of filter cake and mud invasion particles can alter pore structure and the pore surface area available for interaction with the treatment fluids (e.g. chelating agent solution). Thus, there is a need for further investigation of the secondary formation damage considering the effect of surface area of the rock pores. The objective of this work is to investigate the interactions of the chelating fluids with rock samples in the presence of filter cake

particles using the workflow presented in Fig. 1. The effect of the extent of primary damage on secondary damage is also investigated in this study.

2. Experimental

2.1. Materials

In order to achieve the objectives of this work, four different rock samples (sandstone and carbonate rock samples) were used. The chemical compositions of rock samples are shown in Tables 1 and 2. The primary properties of the rock samples including the diameter, length, porosity and permeability are listed in Table 3.

Water-based barite mud was utilized to deposit filter cake at the top of each core sample. The description for the barite mud ingredients is summarized in Table 4 (Bageri et al., 2017). The barite served as a weighting material in the drilling fluid, while the main function of bentonite clay was to improve the hole cleaning. The median size values (D_{50}) of the used API barite and bentonite particles were 17.5 and 10.1 μm, respectively. XC-polymer was used as viscosifier and BARANEX as a filtration control agent. The salts including KCl, KOH, NaCl, Na_2SO_3, and $CaCO_3$ were used as clay controller, pH controller, oxygen scavenger, and as bridging material, respectively. The solids including Soltex, and BlackNite, were added to enhance the filtration properties and stabilize shale, while SOURSCAV was used as H_2S scavenger (Bageri et al., 2017). The mud has a density of 119 Ib/ft^3 and plastic viscosity of 34 cP.

A filter cake removal treatment solution consisting of a chelating agent (20 wt% DTPA) and converting agent (6 wt%) was used (Bageri et al., 2017).

2.2. Experimental methods

A series of experiments was conducted to study formation damage including HPHT fluid loss and removal tests (using HPHT filter press cell from OFITE), solubility tests (using multiple-position hot plate stirrer) and core flooding tests (using FDES645Z Coretest core flooding system). Moreover, NMR relaxometry technique (using Geospec 2.1 rock analyzer from Oxford instrument) was conducted to evaluate the structure of the rock sample at different stages.

In Step 1, barite mud (Table 4) was loaded in the HPHT fluid loss cell at the top of the different rock samples (Table 3) to form a filter cake. The filter cake was formed at a differential pressure of 300 psi and 150 °F. This introduces damage into the core since there will be particle invasion. Prior to filter cake formation, the cores were saturated with brine (i.e., 3% of KCl) and the liquid permeability was measured using the core flooding system. Various injection rates (i.e., 2, 1, and 0.5 mL/min) were utilized to estimate the core liquid permeability. The filter cake was wiped carefully after drying for few hours using a sharp edge tool.

In step 2, the barite particles were dissolved in the removal fluid (chelating agent solution) using the solubility apparatus. It was placed at 270 °F for 24 h to assure that the chelating agent is saturated with barium. By plotting the rate vs. pressure drop, the

Table 1
Chemical composition of sandstone rock samples.

Mineral	Content, %
SiO_2	93.2
Al_2O_3	3.9
FeO	0.5
MgO	0.4
Other impurities	2.0

Table 2
Chemical composition of carbonate rock samples.

Mineral	Content, %
$CaCO_3$	97.0
SiO_2	1.6
Al_2O_3	0.5
$MgCO_3$	0.4
Other impurities	0.5

permeability can be estimated using Darcy's law.

Finally, the prepared solution in Step 2 (chelating agent solution saturated with barium) was injected into the rock samples that had been invaded by mud particles (primary damage, Step-1) using the core flooding experiment which has been listed as Step 3.

The core flooding system consists of main parts including a core holder, accumulators, a sample collector, injection and overburden pressure pumps, a heating oven, a recording and acquisition system The core flooding system was heated first to 212 °F for 4 h to reach the thermal equilibrium and the backpressure was set to be 1000 psi to ensure a constant pore pressure of 1000 psi. Initially, two PV of chelating agent solution was injected into the rock sample at a low rate of 0.25 mL/min. After that, both the inlet and outlet of the core were closed for 24 h to induce interaction. The permeability was measured again using the KCl brine after the ageing process.

3. Results and discussion

The primary damage (Step 1) is an essential step for attaining a reliable downhole process. However, the presence of this step kept the complexity of the formation damage perception mechanisms by altering the surface area and pore structure. This section is divided into the following three subsections.

3.1. Sandstone samples

Fig. 2a compares the pore size distribution based on NMR T_2 distribution (NMR-PSD) for Sample A (sandstone) before and after primary damage (Stage 1). The green curve represents the NMR measurement for the core sample at the initial state (100% brine saturated) while the red curve represents the pore size distribution of the core after solids invasion. The red shaded region demonstrates the volume of the pores occupied by the invaded mud particles located in the macropores (at T_2 values greater than 40 ms). The porosity change due to particle invasion is 2.3% as shown in Table 5.

Following mud solid invasion, the core sample was placed in the core flooding apparatus to investigate the interaction between the chelating agent solution (saturated with barium) and the core sample. The pore size distribution of the rock after 24 h of interaction between the chelating agent and the mud solids (Stage 3) was determined through NMR measurements as shown by the blue curve in Fig. 2b. The light blue shaded region represents the pores that were recovered or cleaned after damage (damage is represented by the red curve). The green shaded region represents the reduced pores due to interacting chelating agent solution with rock samples (with respect to the red curve). The remaining red shaded region represents the permanently damaged pores that could not be recovered by the chelating agent during the 24-h period. The results show that, there is a slight reduction in the number of pores having T_2 values in the range of 0.1—20 ms (green shaded area). Conversely, the number of larger pores that got expanded is in the T_2 range of 40—700 ms (blue shaded area).

The pore structure analysis for the rock sample which has similar properties to Sample A before and after the interaction with

Table 3
Properties of core samples.

Sample ID	Mineralogy	Diameter, cm	Length, cm	Porosity, %	Liquid permeability, mD
Sample A	Sandstone	3.792	4.877	11.4	211
Sample B	Sandstone	3.795	5.029	14.4	0.089
Sample C	Carbonate	3.805	5.024	10.8	0.318
Sample D	Carbonate	3.741	4.806	9.8	0.157

Table 4
Drilling fluid formulation.

Name	Unit	Description
Water	bbl.	0.691
Bentonite	lb.	4
XC-polymer	lb.	0.5
BARANEX	lb.	0.25–0.50
KCl	lb.	20.0
KOH	lb.	0.5
NaCl	lb.	66
Barite	lb.	352.0
$CaCO_3$ medium	lb.	5.0
Sodium sulfite	lb.	0.25–0.30
Soltex	lb.	1.0–2.0
BlackNite	gal	0.3–0.5
SOURSCAV	lb	2

barium-saturated chelating agent is shown in Fig. 2c. It is worth to mention that the interaction methodology was simplified in which the rock sample was not subjected to the primary damage stage (Bageri et al., 2019). The data of this figure was obtained by injecting the chelating agent solution into the sandstone sample using the core flooding apparatus at the same conditions of this study. The green and blue shaded areas represent the reduction and the enlargement in the pores caused by the interaction.

Similarly, Fig. 3 is the result for the second sandstone sample. Fig. 3a shows the NMR-PSD plots for Sample B before and after damage due to mud solid invasion (Stage 1). The volume of the pores occupied by the invaded particles reduced the porosity of the core sample by 3.9% (Table 5). The damage occurred in the pores having T_2 values in the range of >7 ms. Pore size distribution after treatment is shown by the blue curve in Fig. 3b. The areas under the curves shaded with blue represent the recovered pores after treatment. It can be observed in this case that the blue shaded pores exceeded the initial pore size. The excess being in the T_2 region lying between 20 and 150 ms (shaded dark blue). The chelating agent appeared to have dissolved more clay or rock matrix after cleaning up the damage. Fig. 3c presents the secondary damage of the sandstone rock sample that has similar properties of Sample B without subjecting the core to the primary damage stage (Bageri et al., 2019). The interaction took place directly between the rock sample and the saturated barium chelating agent.

In comparison, the primary damage stage in sample (Sample A) showed that porosity occupied by the invaded particles was 2.3% out of an initial core porosity 11.4%, which is approximately equivalent to a 20%. Meanwhile, the estimated porosity reduction for the second sample (Sample B) was 26%. A clear distinction in the primary damage (Stage 1) for samples A and B was observed in the NMR results. The NMR PSD plots show that the solid invasion occurred in T_2 range of $7 < T_2 < 800$ in Sample A, while invaded solids fall in the range of $10 < T_2 < 150$ for Sample B. The area of the red shaded region in both samples could be used to quantify the solid invasion (Bageri et al., 2020). Based on this area, the area in Sample A is relatively four times higher than that in Sample B (78.24 and 19.84 pu·ms, respectively). Furthermore, the increase in the rock sample weight at the end of Stage 1 is another way to
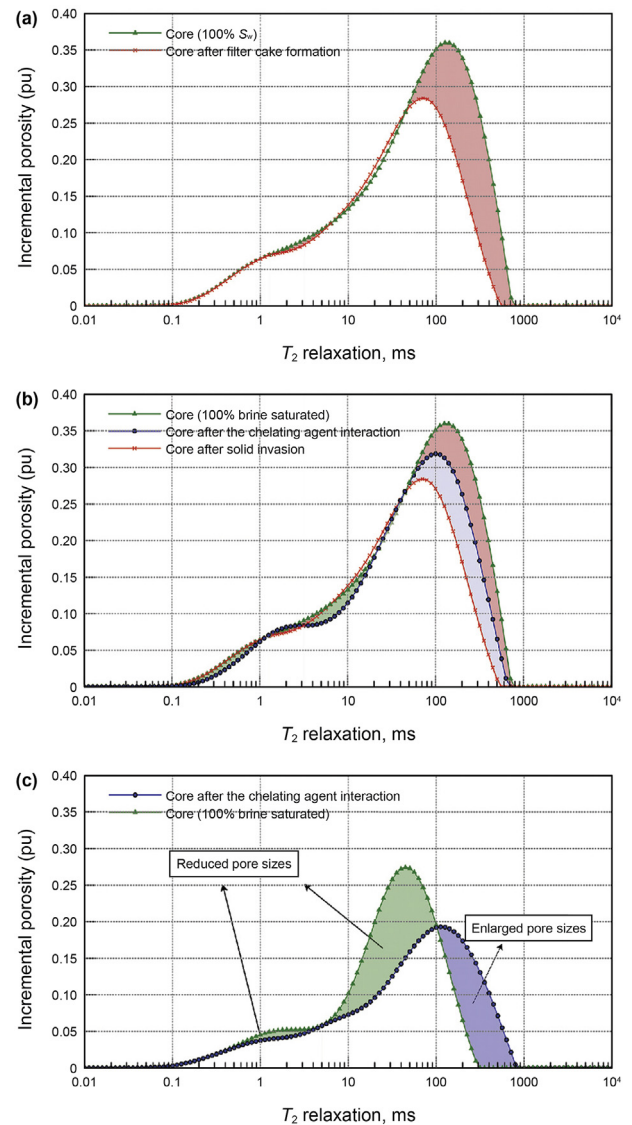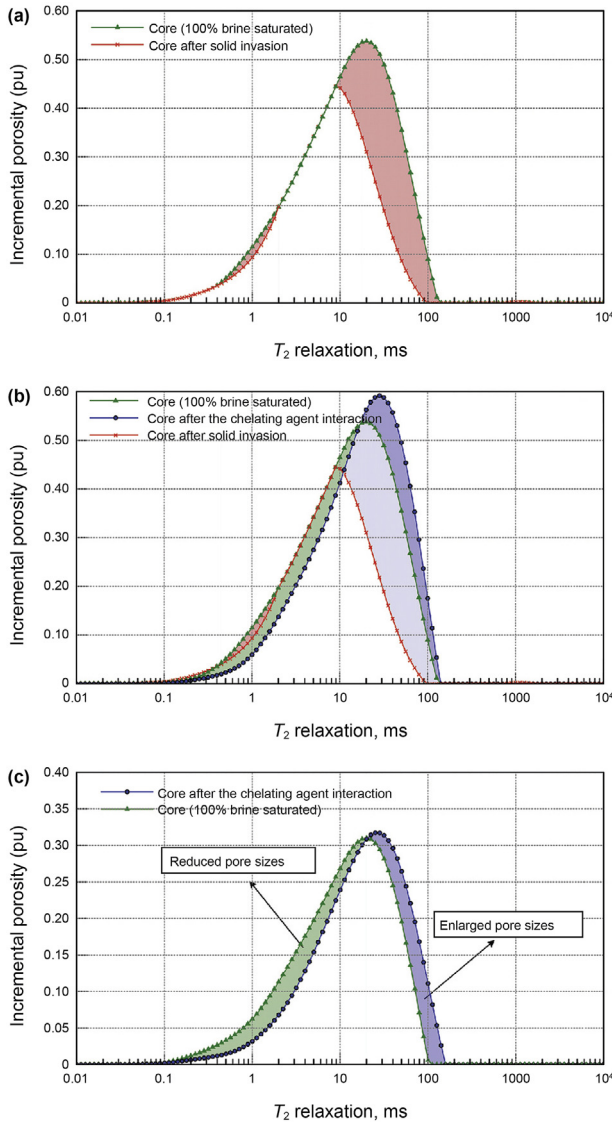

Fig. 2. The incremental porosity obtained by the NMR for Sample A (sandstone) at different stages.

quantify solids invasion. The weight of Sample A increased by 2.37 g while the weight of Sample B increased by 0.87 g. Based on the two indices (the red shaded area and weight), the quantity of the solid particles that invaded Sample A was higher than that in Sample B.

In order to understand the role of primary damage in the interaction between the solvent and rock minerals, the reaction between the injected solvent and the rock mineral has to be compared for the case with damage and the case without primary damage. Figs. 2c and 3c show the post treatment NMR-PSD for the case where the chelating agent interacted with the rock minerals in the absence of primary damage. It appears that the chelating agent

Table 5
The porosity values for each sample from NMR measurements.

Sample ID	Core initial porosity (100% brine saturated) ϕ_i, %	Core porosity after filter cake formation ϕ_1, %	Core porosity after filter cake removal ϕ_f, %	Porosity change in Stage 1 $\phi_i - \phi_1$, %	Porosity change in Stage 2 $\phi_1 - \phi_f$, %	Total change in porosity $\phi_i - \phi_f$, %
Sample A	11.431	9.127	9.889	2.304	−0.762	1.542
Sample B	14.529	10.630	14.433	3.899	−3.803	0.096
Sample C	10.849	10.079	9.275	0.769	0.804	1.574
Sample D	9.881	8.796	9.722	1.085	−0.926	0.159

Fig. 3. The incremental porosity obtained by the NMR for Sample B (sandstone) at different stages.

has similar reactivity behavior with the case where primary damage occurred. The barite-laden chelating agent release the barium in the small pores and becomes partially active to dissolve clay minerals in the large pores as shown in Figs. 2c and 3c. It can be seen in these figures that the barite saturated chelating agent released the barites in the area shaded green in Figs. 2c and 3c and then proceeded to dissolve the matrix to create large pores denoted

by the areas shaded blue.

In Sample A, the partially active chelating agent, after releasing the barium, was not capable of recovering all the damaged pores but only recovered a fraction shown by the primary damage (light blue shaded area in Fig. 2b). However, in Sample B, it was able to recover the damaged pores (light blue) and open new pores (represented by dark blue). Therefore, it may be possible to conclude that the amount of solids that invaded the rock samples and the permeability of cores played a vital role in this process. The solids that invaded Sample A was higher than Sample B as previously discussed. The deposited barite in the large pores during mud invasion may cover the clay minerals and act as a barrier that delays stripping of the clay from the same site. Therefore, the chelating agent was forced to interact with the rock minerals instead, which caused recovery of the plugged pores in both samples and created new or enlarged pores in Sample B. The difference in the level of solids invasion can be justified by the large difference in permeability of samples. The permeability of Sample A is 211 mD while that of Sample B is 0.089 mD, as shown in Table 3.

3.2. Carbonate samples

The results of the carbonate samples (Samples C & D) are shown in Figs. 4 and 5. The results of the first stage showed that the porosity reduced by a ratio of 7% and 11%, respectively, due to solids invasion. Moreover, the PSD ranges affected by the primary damage is located at different sites. In Sample C, the primary damage occurred in pores with T_2 values ranging from 60 to 4000 ms, while the range for Sample D was from 30 to 2000 ms. The area of the damaged zone (red shade) is estimated for Sample C to be 107.42 pu·ms and for Sample D to be 17.44 pu·ms. Based on weight of the invaded solids, the invaded solids in Sample C weigh 2.61 g while they weigh 0.19 g in samples D. Hence, the primary damage was more severe in Sample C than in Sample D.

In the case of carbonate samples, the barite-laden chelating agent released its barite in the large pores (as opposed to the small pores in sandstones) and substituted it with cations (i.e., calcium cation) extracted from the smaller pores. This phenomenon is shown in Figs. 4c and 5c (for the case where primary damage was not present (Bageri et al., 2019)) and in Figs. 4b and 5b (for the case with primary formation damage). The difference between the two cases is that, for the case where primary damage occurred, the invaded particles (barites) served as a diverter for the flowing chelating agent so that it invaded both the small and large pores at the same time. It was shown in a previous study that the chelating agent solution flowed easily in the large pores and hence released its barite in the same site (large pores). In this present case (post primary damage), the active chelating agent was diverted to and reacted with the calcite in the smaller pores since the large pores were partially occupied by the invaded solid.
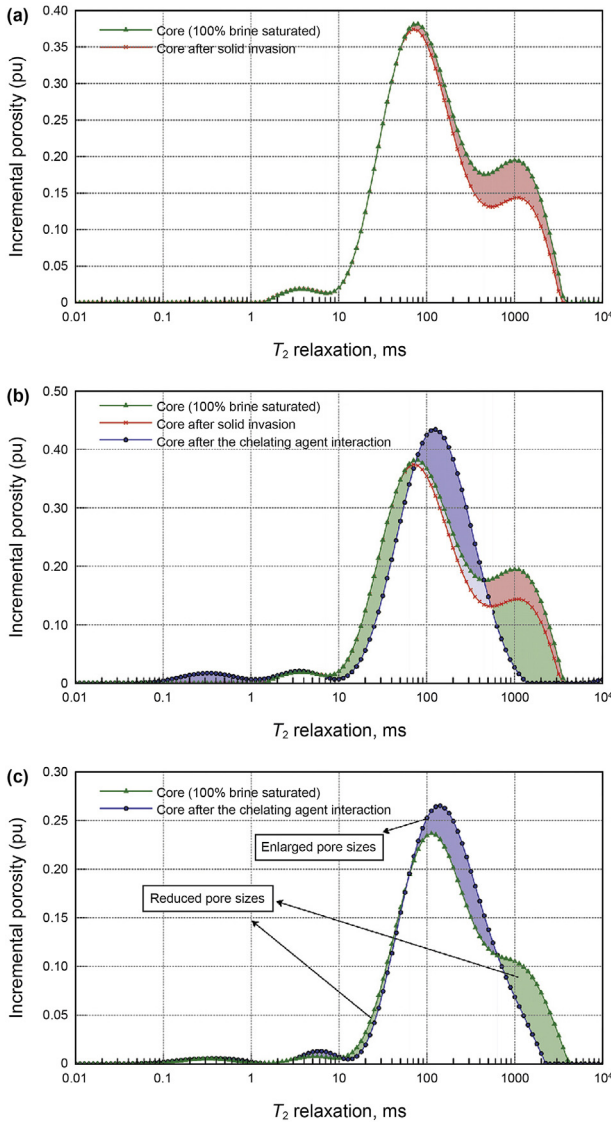
Fig. 4. The incremental porosity obtained by the NMR for carbonate sample (Sample C) at different stages.

Fig. 5. The incremental porosity obtained by the NMR for carbonate sample (Sample D) at different stages.

3.3. Comparison

The need for this comparison between the case of primary formation damage and the case where there is no primary formation damage is to promote better understating of the role of primary damage. The first index is obtained by relating the reduction of pores with the enlargement of pores (all occurring during the treatment process) as shown in Fig. 6. The two cases are represented in this figure. A 45-degree line is drawn to highlight where the pore reduction is equal to pore enlargement, or better put as, where the amount of barite released by the chelating agent is equal to the number of new cations absorbed by the chelating agent. This index reflects reaction and precipitation rates during the entire process. In general, the data points are located around the 45-degree line. This indicates that the reaction rate of the chelating agent was mostly equal to the drop rate of the barium during the secondary damage. The red data points represent the case where reaction took place in the presence of primary damage stage, while the green data points represent the other case (no primary damage). The data points in red (presence of primary damage) are
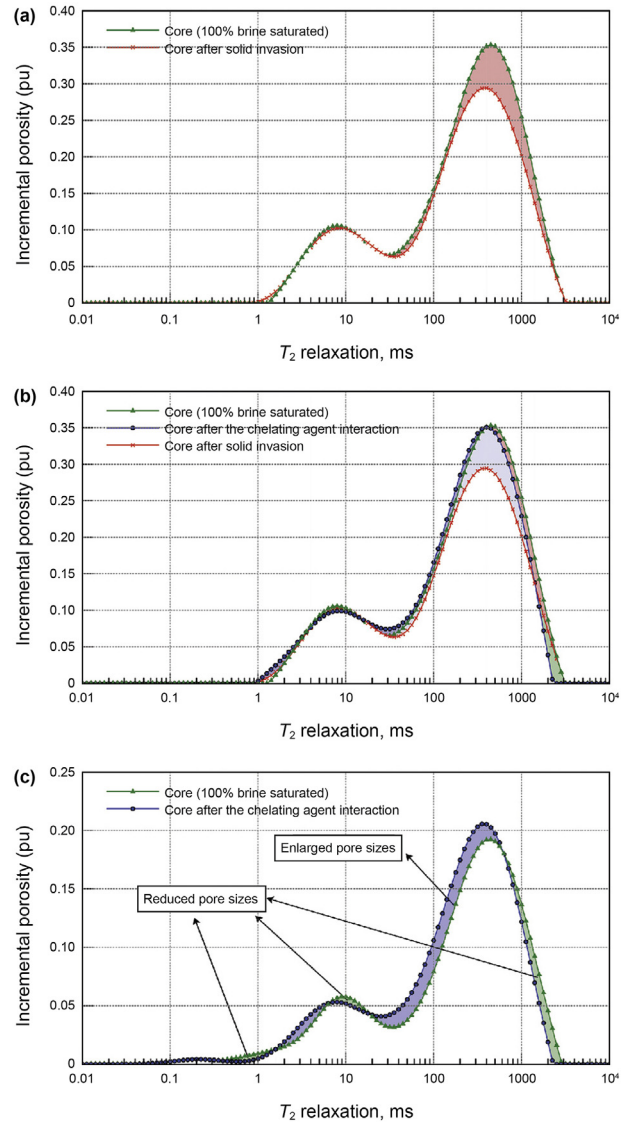
exposed to two stages of barite precipitation - first, during the mud solids invasion and then during secondary damage. The points with similar shape present the same rock sample in the different cases with and without primary damage. The least squares fit on the green data points is overlapping the 45-degree line. The red line is a least squares fit on the red point (primary damage case). The more severe the primary damage, the larger is the shift of the data points from the 45-degree line. Hence, the distance between the red line and the 45-degree line represents the degree of damage that cannot be recovered after treatment.

From a practical perspective, the precipitation of solids during both primary and secondary damage stages has to be evaluated in simple measurable terms. Hence, another index was introduced to present the information in a way that is directly relevant to the well productivity. We therefore related the permeability ratio (K_f/K_i) to the porosity ratio (ϕ_f/ϕ_i) whose parameters are obtained at the initial and final stages. The ratios can indicate the status of the rock sample after damage. A ratio greater than one implies an improvement while a ratio less than one implies damage, and a ratio equal to zero means there is no change.
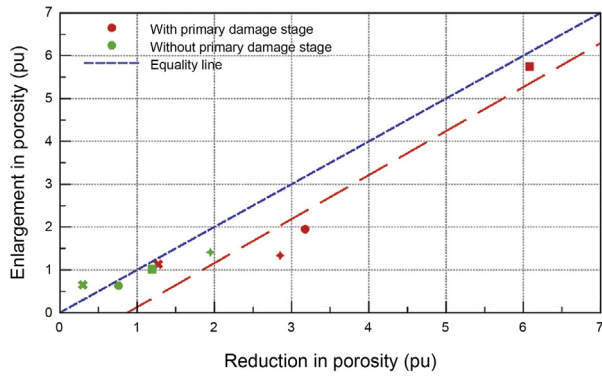
Fig. 6. Reduction versus enlargement of porosiy after the chelating agent interactions with sandstone and carbonate samples.
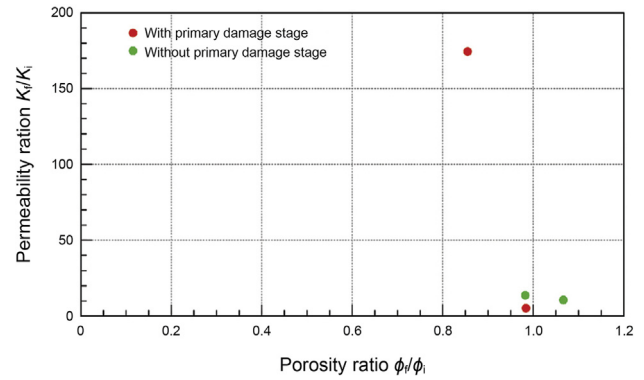

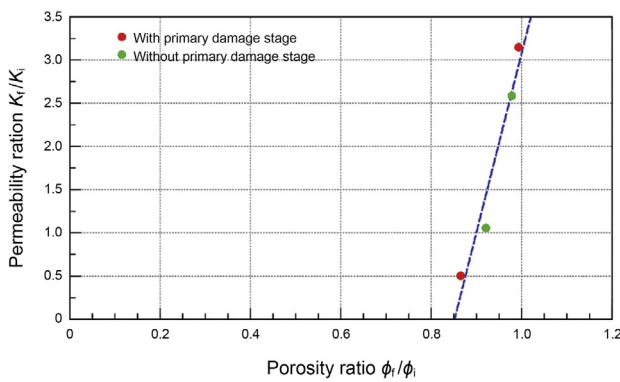**Fig. 8.** Porosity ratio versus the permeability ratio for the carbonate samples.

Fig. 7. Porosity ratio versus the permebailty ratio for the sandstone samples.

As shown in Figs. 7 and 8, the permeability ratio (K_f / K_i) is higher than one for all carbonate and sandstone samples except for one sample. The permeability ratio of sandstone samples reached a value as high as 3. This fact can be attributed to the reaction of chelating agent with sandstone in which the reaction is limited only to the clay mineral existing in the pores and controlled by their stability constant (Bageri et al., 2019; Fredd and Fogler, 1998). Thus, the higher amount of the clay minerals dissolved by the chelating agent (indicated by higher porosity ratio) relatively yielded a higher improvement in the permeability as shown in Fig. 7. In carbonate samples, the chelating agent has the capability to open wormholes because it reacts with the carbonate matrix (Barri et al., 2016), thus the ratio of (K_f/K_i) showed high value in one sample (175 times improvement) as shown in Fig. 8. In the other three carbonate samples, the partially active chelating agent lost its capability of creating such wormholes, and as such the permeability ratio increased 15 times. Another interesting observation in the majority of the tested samples in both cases (i.e., with and without primary damage) is the reduction in the porosity ratio (ϕ_f/ϕ_i), except one sample.

4. Conclusions

The filter cake formation and removal processes can result in two different types of damage: the primary damage caused by the solids invasion and the secondary damage caused by the interaction of the chelating agent (removal solvent) with formation rock samples. An experimental study using NMR was conducted to verify the effect of the primary damage on the secondary damage. The main findings of this work are:

(1) During the filter cake removal process, the barite-laden chelating agent discharged the barium particles in the small pores (secondary damage) and subsequently absorbed clay minerals from other pore sites in the sandstone samples. The results have shown that the primary damage can be effectively controlled by the chelating agent reactivity with the formation rock samples after the filter cake removal process. Higher concentration of barium in the macropores during the primary damage tend to divert the chelating agent into small pores, where it drops the barium, resulting in the secondary damage.

(2) In carbonate samples, the simplified scenario ignoring the primary damage stage showed that the barite-laden chelating agent absorbed the metallic ions from the small pores and released the barium in the large pores. The loaded barium during the primary damage served as the divergent point for the chelating agent to invade both pore systems. The loaded barium constrained the flow in the large pores, which forced the barite-laden chelating agent to flow in the small pores that have high content of the metallic ions (i.e., calcium cation). The metallic ions triggered the exchange process of the ions, hence the chelating agent restored part of its reactivity to react and expand the pores.

(3) The reaction rate of the chelating agent in both sandstone and carbonate rock samples is mostly equal (i.e., overlapping the 45-degree line) to the precipitation rate of the barium during the secondary damage. The higher the intensity of the primary damage, the larger the shift from the 45-degree line.

Regardless of the improvement that might result from the chelating agent reaction, the additional precipitation of barium might cause negative impact on the environment and the general health. Therefore, the authors emphasize the importance of minimizing both damages as possible; the primary damage by using the suitable bridging material (i.e., size and concentration) and the secondary damage by performing the removal process at the minimal differential (zero) pressure.

References

Adebayo, A.R., Bageri, B.S., 2019. A simple NMR methodology for evaluating filter cake properties and drilling fluid-induced formation damage. J. Pet. Explor. Prod. Technol. 10 (4), 1643–1655. https://doi.org/10.1007/s13202-019-00786-3.

Adebayo, A.R.A.R., Bageri, B.S.B.S., Al Jaberi, J., Salin, R.B.R.B., 2020. A calibration method for estimating mudcake thickness and porosity using NMR data. J. Pet. Sci. Eng. 195 (June), 107582. https://doi.org/10.1016/j.petrol.2020.107582.

Ahmad, H.M., Kamal, M.S., Al-Harthi, M.A., 2018. High molecular weight copolymers as rheology modifier and fluid loss additive for water-based drilling fluids. Jouranl Mol. Liq. 252, 133–143. https://doi.org/10.1016/j.molliq.2017.12.135.

Al Jaberi, J., Bageri, B.S., Barri, A., Adebayo, A., Patil, S., Babu, R., et al., 2020. Insight into secondary posterior formation damage during barite filter cake removal in calcite formations. In: International Petroleum Technology Conference, January 13–15. https://doi.org/10.2523/IPTC-19611-MS.

Al Moajil, A.M., Nasr-El-Din, H.A., 2011. Formation damage caused by improper Mn_3O_4-based filter cake cleanup treatments. In: SPE European Formation Damage Conference, June 7–10. https://doi.org/10.2118/144179-MS.

Al Moajil, A.M., Nasr-El-Din, H.A., 2013. Formation damage caused by improper Mn_3O_4-based filter-cake-cleanup treatments. J. Can. Pet. Technol. 52 (1), 64–74. https://doi.org/10.2118/144179-PA.

Al Moajil, A.M., Nasr-El-Din, H.A., 2014. Removal of manganese tetraoxide filter cake using a combination of HCl and organic acid. J. Can. Pet. Technol. 53 (2), 122–130. https://doi.org/10.2118/165551-PA.

Al Moajil, A., Nasr-El-Din, H.A., Al-Yami, A., Al-Aamri, A., Al-Aqil, A., 2008. Removal of filter cake formed by manganese tetraoxide based-drilling fluids. In: SPE Int. Symp. Exhib. Form. Damage Control. Lafayette, Louisiana, USA, 13-15 Febr. https://doi.org/10.2118/112450-MS.

Al Otaibi, M.B., Nasr-El-Din, H.A., Hill, A.D., 2008. Characteristics and removal of filter cake formed by formate-based drilling mud. In: SPE International Symposium and Exhibition on Formation Damage Control, February 13–15. https://doi.org/10.2118/112427-MS.

Al-Mutairi, S.H., Al-Dhufairi, M.A., June 2010. Lessons learned from stimulation treatments and filter cake removal practices in high permeability carbonate during the drilling phase. In: International Oil and Gas Conference and Exhibition in China, Beijing, China. https://doi.org/10.2118/131869-MS.

Al-Yaseri, A.Z., Lebedev, M., Vogt, S.J., Johns, M.L., Barifcani, A., Iglauer, S., 2015. Pore-scale analysis of formation damage in Bentheimer sandstone with in-situ NMR and micro-computed tomography experiments. J. Pet. Sci. Eng. 129, 48–57. https://doi.org/10.1016/j.petrol.2015.01.018.

Bageri, B.S., Adebayo, A.R., Al Jaberi, J., Patil, S., 2020. Effect of perlite particles on the filtration properties of high-density barite weighted water-based drilling fluid. Powder Technol 360, 1157–1166. https://doi.org/10.1016/j.powtec.2019.11.030.

Bageri, B.S., Adebayo, A.R.R., Barri, A., Al Jaberi, J., Patil, S., Hussaini, S.R., et al., 2019. Evaluation of secondary formation damage caused by the interaction of chelated barite with formation rocks during filter cake removal. J. Pet. Sci. Eng. 183. https://doi.org/10.1016/j.petrol.2019.106395, 2019.

Bageri, B.S., Al-Mutairi, S.H., Mahmoud, M.A., 2013. Different techniques for characterizing the filter cake. In: SPE Unconventional Gas Conference and Exhibition, January 28–30. https://doi.org/10.2118/163960-MS.

Bageri, B.S., Mahmoud, M., Abdulraheem, A., Al-Mutairi, S.H., Elkatatny, S.M., Shawabkeh, R.A., 2017. Single stage filter cake removal of barite weighted water based drilling fluid. J. Pet. Sci. Eng. 149, 476–484. https://doi.org/10.1016/j.petrol.2016.10.059.

Bageri, B.S., Mahmoud, M.A., 2013. A new diversion technique to remove the formation damage from maximum reservoir contact and extended reach wells in sandstone reservoirs. In: SPE European Formation Damage Conference & Exhibition, June 5–7. https://doi.org/10.2118/165163-MS.

Barri, A., Mahmoud, M., Elkatatny, S., 2016. Evaluation of rock mechanical properties alteration during matrix stimulation with chelating agents. J. Energy Resour. Technol. Trans. ASME. 138 (3), 1–7. https://doi.org/10.1115/1.4032546.

Basnayaka, L., Subasinghe, N., Albijanic, B., 2018. Influence of clays on fine particle filtration. Appl. Clay Sci. 45–52. https://doi.org/10.1016/j.clay.2018.01.008.

Byrne, M.T., Patey, I.T.M., Twynam, A.J., 2000. Laboratory drilling mud overbalance formation damage study utilising cryogenic SEM techniques. In: SPE International Symposium on Formation Damage Control, February 23–24. https://doi.org/10.2118/58738-MS.

Ding, Y., Liu, X.J., Luo, P.Y., 2020. Investigation on influence of drilling unloading on wellbore stability in clay shale formation. Pet. Sci. 17 (3), 781–796. https://doi.org/10.1007/s12182-020-00438-w.

Elkatatny, S.M., Mahmoud, M.A., Nasr-El-Din, H.A., 2011. A new approach to determine filter cake properties of water-based drilling fluids. In: SPE/DGS Saudi Arabia Section Technical Symposium and Exhibition, May 15–18. https://doi.org/10.2118/149041-MS.

Elsayed, M., Mahmoud, M., El-Husseiny, A., Kamal, M.S., Al-Garadi, K., 2020. A new method to evaluate reaction kinetics of acids with carbonate rocks using NMR diffusion measurements. Energy and Fuels 34 (1), 787–797. https://doi.org/10.1021/acs.energyfuels.9b03784.

Ettehadi, A., Altun, G., 2017. Extending thermal stability of calcium carbonate pills using sepiolite drilling fluid. Pet. Explor. Dev. 44 (3), 477–486. https://doi.org/10.1016/S1876-3804(17)30055-1.

Fattah, K.A., Lashin, A., 2016. Investigation of mud density and weighting materials effect on drilling fluid filter cake properties and formation damage. J. African Earth Sci. 117, 345–357. https://doi.org/10.1016/j.jafrearsci.2016.02.003.

Fredd, C.N., Fogler, H.S., 1998. The influence of chelating agents on the kinetics of calcite dissolution. J. Colloid Interface Sci. 204 (1), 187–197. https://doi.org/10.1006/jcis.1998.5535.

Green, J., Cameron, R., Patey, I., Nagassar, V., Quine, M., 2013. Use of micro-CT scanning visualisations to improve interpretation of formation damage laboratory tests including a case study from the south morecambe field. In: SPE European Formation Damage Conference & Exhibition, June 5–7. https://doi.org/10.2118/165110-MS.

Guancheng, J., Xiaoxiao, H., Wuquan, L., Xiaohu, Q., Xuwu, L., 2020. Super-amphiphobic, strong self-cleaning and high-efficiency water-based drilling fluids. Pet. Explor. Dev. 47 (2), 421–429. https://doi.org/10.1016/S1876-3804(20)60059-3.

Hodge, R.M., Augustine, B.G., Burton, R.C., Sanders, W., Stomp, D.A., 1997. Evaluation and selection of drill-in-fluid candidates to minimize formation damage. SPE Drill. Complet. 12 (3), 174–179. https://doi.org/10.2118/31082-PA.

Hossain, M.E.M., Al-Majed, A.A.A., 2015. Fundamentals of Sustainable Drilling Engineering. Scrivener Publ. Wiley.

Iscan, A.G., Civan, F., Kok, M.V., 2007. Alteration of permeability by drilling fluid invasion and flow reversal. J. Pet. Sci. Eng. 58 (1–2), 227–244. https://doi.org/10.1016/j.petrol.2007.01.002.

Khodja, M., Canselier, J.P., Bergaya, F., Fourar, K., Khodja, M., Cohaut, N., et al., 2010. Shale problems and water-based drilling fluid optimisation in the Hassi Messaoud Algerian oil field. Appl. Clay Sci. 383–393. https://doi.org/10.1016/j.clay.2010.06.008.

Liu, B., Cheng, S., Nie, X., Zhao, Y., 2013. Evaluation of damage to horizontal wells through equivalent horizontal well length. Pet. Explor. Dev. 40 (3), 378–382. https://doi.org/10.1016/S1876-3804(13)60046-4.

Mahmoud, M., 2019. Well clean-up using a combined thermochemical/chelating agent fluids. J. Energy Resour. Technol. Trans. ASME. 141 (10), 102905. https://doi.org/10.1115/1.4043612.

Mahmoud, M., Bageri, B.S., Elkatatny, S., Al-Mutairi, S.H., 2017. Modeling of filter cake composition in maximum reservoir contact and extended reach horizontal wells in sandstone reservoirs. J. Energy Resour. Technol. 139 (3), 032904. https://doi.org/10.1115/1.4035022.

Mahmoud, M.A., Bageri, B.S., Abdelgawad, K., Kamal, S.M., Hussein, I., Elkatantny, S., et al., 2018a. Evaluation of the reaction kinetics of diethylenetriaminepentaacetic acid chelating agent and a converter with barium sulfate (barite) using a rotating disk Apparatus. Energy & Fuels 32 (9), 9813–9821. http://pubs.acs.org/doi/10.1021/acs.energyfuels.8b02332.

Mahmoud, O., Nasr-El-Din, H.A., Vryzas, Z., Kelessidis, V.C., 2018b. Effect of ferric oxide nanoparticles on the properties of filter cake formed by calcium bentonite-based drilling muds. SPE Drill. Complet. 33 (4), 363–376. https://doi.org/10.2118/184572-PA.

Mao, H., Yang, Y., Zhang, H., Zheng, J., Zhong, Y., 2020. Conceptual design and methodology for rheological control of water-based drilling fluids in ultra-high temperature and ultra-high pressure drilling applications. J. Pet. Sci. Eng. 188 (1), 106884. https://doi.org/10.1016/j.petrol.2019.106884.

Nasr-El-Din, H.A., 2005. Formation damage induced by chemical treatments: case histories. J. Energy Resour. Technol. 127 (3), 214. https://doi.org/10.1115/1.1924464.

Nunes, M., Bedrikovetsky, P., Newbery, B., Paiva, R., Furtado, C., De Souza, A.L., 2010. Theoretical definition of formation damage zone with applications to well stimulation. J. Energy Resour. Technol. 132 (3), 033101. https://doi.org/10.1115/1.4001800.

Qiansheng, Y., Shujie, L., Xingjin, X., 2010. Drilling fluid technology for horizontal wells to protect the formations in unconsolidated sandstone heavy oil reservoirs. Pet. Explor. Dev. 37 (2), 232–236. https://doi.org/10.1016/S1876-3804(10)60029-8.

Siddiqui, M.A., Nasr-El-Din, H.A., 2003. Evaluation of special enzymes as a means to remove formation damage induced by drill-in fluids in horizontal gas wells in tight reservoirs. In: SPE Middle East Oil Show. https://doi.org/10.2118/81455-MS. June 9–12.

Smith, S.R., Rafati, R., Sharifi Haddad, A., Cooper, A., Hamidi, H., 2018. Application of aluminium oxide nanoparticles to enhance rheological and filtration properties of water based muds at HPHT conditions. Colloids Surfaces A Physicochem. Eng. Asp. 537 (September 2017), 361–371. https://doi.org/10.1016/j.colsurfa.2017.10.050.

Sun, J., Huang, X., Jiang, G., Lyu, K., Liu, J., Dai, Z., 2018. Development of key additives for organoclay-free oil-based drilling mud and system performance evaluation. Pet. Explor. Dev. 45 (4), 764–769. https://doi.org/10.1016/S1876-3804(18)30079-X.

Wanderley Neto, A.O., da Silva, V.L., Rodrigues, D.V., Ribeiro, L.S., Nunes da Silva, D.N., de Oliveira Freitas, J.C., 2020. A novel oil-in-water microemulsion as a cementation flushing fluid for removing non-aqueous filter cake. J. Pet. Sci. Eng. https://doi.org/10.1016/j.petrol.2019.106536.

Wang, F., Tan, X., Wang, R., Sun, M., Wang, L., Liu, J., 2012. High temperature and high pressure rheological properties of high-density water-based drilling fluids for deep wells. Pet. Sci. 9 (3), 354–362. https://doi.org/10.1007/s12182-012-0219-4.

Yue, Q., Ma, B., 2008. Development and applications of solids-free oil-in-water drilling fluids. Pet. Sci. 5 (2), 153–158. https://doi.org/10.1007/s12182-008-0023-3.

Zhang, H., Yan, J., Lu, Y., Shu, Y., Zhao, S., 2009. Experimental study of low-damage drilling fluid to minimize waterblocking of low-permeability gas reservoirs. Pet. Sci. 6 (3), 271–276. https://doi.org/10.1007/s12182-009-0043-7.

Zhao, X., Qiu, Z., Sun, B., Liu, S., Xing, X., Wang, M., 2019. Formation damage mechanisms associated with drilling and completion fluids for deepwater reservoirs. J. Pet. Sci. Eng. 173 (66), 112–121. https://doi.org/10.1016/j.petrol.2018.09.098.

Zhong, H., Shen, G., Qiu, Z., Lin, Y., Fan, L., Xing, X., et al., 2019. Minimizing the HTHP filtration loss of oil-based drilling fluid with swellable polymer microspheres. J. Pet. Sci. Eng. 172, 411–424. https://doi.org/10.1016/j.petrol.2018.09.074.